Draft version October 24, 2016
Preprint typeset using LaTeX style emulateapj v. 5/2/11

arXiv:1607.04891v2 [astro-ph.EP] 21 Oct 2016

# PLANETARY ENGULFMENT AS A TRIGGER FOR WHITE DWARF POLLUTION

Cristobal Petrovich[1,2] & Diego J. Muñoz[3]

*Draft version October 24, 2016*

## ABSTRACT

The presence of a planetary system can shield a planetesimal disk from the secular gravitational perturbations due to distant outer massive objects (planets or stellar companions). As the host star evolves off the main sequence to become a white dwarf, these planets can be engulfed during the giant phase, triggering secular instabilities and leading to the tidal disruptions of small rocky bodies. These disrupted bodies can feed the white dwarfs with rocky material and possibly explain the high-metallicity material in their atmospheres. We illustrate how this mechanism can operate when the gravitational perturbations are due to the KL mechanism from a stellar binary companion, a process that is activated only after the planet has been removed/engulfed. We show that this mechanism can explain the observed accretion rates if: (1) the planetary engulfment happens fast compared to the secular timescale, which is generally the case for wide binaries ($> 100$ AU) and planetary engulfment during the Asymptotic Giant Branch ; (2) the planetesimal disk has a total mass of $\sim 10^{-4}-10^{-2} M_{\oplus}$. We show that this new mechanism can provide a steady supply of material throughout the entire life of the white dwarfs for all cooling ages and can account for a large fraction (up to nearly half) of the observed polluted WDs.

## 1. INTRODUCTION

Atmospheric metals are not expected to be present in isolated white dwarfs (WDs) with effective temperatures below $\sim 25,000$ K. At these temperatures, radiative forces become too weak (Chayer et al. 1995) to significantly counteract the quick gravitational settling that sinks material heavier than helium in extremely short timescales compared to the typical cooling ages of WDs (Fontaine & Michaud 1979; Koester 2009). However, it has been found that $\sim 25\%-50\%$ of all field WDs exhibit spectral lines that are indicative of the presence of metals in their atmospheres (Zuckerman et al. 2003, 2010; Koester et al. 2014).

The high-metallicity material found in the atmospheres of most of these "polluted" WDs is consistent with the composition of rock-forming material (Zuckerman et al. 2007; Gänsicke et al. 2012; Farihi et al. 2013; Jura & Young 2014). This observation suggesting that pollution comes from minor rocky bodies (e.g., asteroids). One possibility is that these rocky bodies get very close to the WD so they can be tidally disrupted and then accreted. Further support of this picture comes from observations of circumstellar disks –revealed by infrared excess in the stellar spectrum– around many polluted WDs (see Farihi 2016 for a recent review). These disks orbit within $\sim 1 R_{\odot}$, roughly the distance at which the material would reside after the tidal disruption (the Roche radius). All the WDs with detected disks have atmospheric pollution. More recently, this picture has been reinforced by the recent observation of minor bodies transiting the polluted WD 1145+017 (Vanderburg et al. 2015; Alonso et al. 2016; Gänsicke et al. 2012; Rappaport et al. 2016; Xu et al. 2016).

Although the leading explanation for WDs pollution –the accretion of tidally disrupted asteroids– seems robust and well supported by observations, the underlying dynamical mechanism responsible for placing these rocky bodies in star grazing orbits remains much less constrained and understood. A better understanding of this mechanism can lead to new insights into initial conditions leading to WD pollution, as well as into the long-term dynamics and evolution of the planetary systems around WDs and/or their progenitors (typically A and F stars; see Veras 2016 for a recent review on this subject).

A theoretical model to explain the WD pollution from planetary dynamical instabilities was put forward by Debes & Sigurdsson (2002). According to their model, a planetary system that is marginally stable throughout the main sequence can become unstable due to stellar mass loss during post-MS evolution. This global instability can then promote some asteroids into star grazing orbits. This idea has been explored in more detail using realistic numerical $N$-body integrations of multi-planet systems (no asteroids) and stellar evolution (Veras et al. 2013; Mustill et al. 2012; Veras & Gänsicke 2015). Similarly, the mass loss of the host star can widen the region around mean-motion resonances where chaotic diffusion of asteroids acts efficiently, leading to their posterior tidal disruption (Bonsor et al. 2011; Debes et al. 2012; Frewen & Hansen 2014). As well, mass loss in close binary systems can drive the outermost planetesimals into the chaotic orbits, with one of the possible outcomes being collisions with either one of the stars (Kratter & Perets 2012).

Thus far, these proposed dynamical mechanisms rely on generally short-timescale instabilities (either scattering or mean-motion-resonance overlap) triggered (or en-

[1] Canadian Institute for Theoretical Astrophysics, University of Toronto, 60 St George Street, ON M5S 3H8, Canada; cpetrovi@cita.utoronto.ca
[2] Centre for Planetary Sciences, Department of Physical & Environmental Sciences, University of Toronto at Scarborough, Toronto, Ontario M1C 1A4, Canada
[3] Cornell Center for Astrophysics and Planetary Science, Department of Astronomy, Cornell University, Ithaca, NY 14853, USA

hanced) by mass loss or simply by the aging of the planetary systems, and still face some difficulties. In particular, these mechanisms are subject to the following constraints:

1. *the delivery of material must happen for WDs of all ages.*

   The observations seem to show that neither the rate of polluted WDs, nor that the level of pollution decreases with the WD cooling age (Koester et al. 2014; Wyatt et al. 2014). Thus, to explain the observed pollution rate, the underlying mechanism should be able to deliver enough material into the WD's atmosphere independently of how much time it has passed since the stellar mass loss phase.

2. *The supply of material into white dwarf grazing orbits must be a steady process.*

   Both the large observed rate of polluted WDs and the short timescales that follow a disruption event (or order the orbital timescale) require of a sustained process to deliver bodies toward disruption. The formation of a debris disks following disruption can extend the duration of the delivery toward the stellar atmosphere, but its associated timescale is still short compared to the cooling ages of most polluted WDs (Veras et al. 2014, 2015).

3. *The reservoir of rocky material has to be long-lived.*

   The amount of material waiting to be delivered toward the star cannot be arbitrarily large. A planetesimal disk can be destroyed by a collisional cascade, shattering the rocky bodies down to dust, which can be blown out during the RG and AGB phases by radiation pressure (e.g., Bonsor & Wyatt 2010). All else being equal, disks with lower surface densities and at larger separations can survive for longer timescales, possibly avoiding this fate (e.g., Wyatt et al. 2007; Heng & Tremaine 2010; Bonsor & Wyatt 2010).

In this paper, we propose a new mechanism that overcomes (or at least alleviates) these difficulties.

We propose that the nature of the instabilities, which drives the material in a planetesimal disk into disrupting orbits, is secular (not scattering nor driven by mean-motion resonances) and that the instabilities are initiated only at the very end of the the stellar evolution (AGB phase) once a stabilizing, pre-existing planetary system is engulfed by an extended stellar envelope. This mechanism can provide steady pollution over all ages of the WD (overcoming the difficulties 1 and 2), while working for a low surface density disk that remains dynamically cold during the main sequence, and that gets gradually depleted long after mass loss has taken place (addressing difficulty 3).

We illustrate how the instabilities arise due to the Kozai-Lidov (KL) mechanism in wide ($\gtrsim$ 100 AU) stellar binaries, although our proposal is more general and sub-stellar companions and other sources of secular excitation are allowed. We expect that for these wide binaries the possible WD pollution associated with post-AGB dust disks and stellar winds might be negligible (e.g., De Ruyter et al. 2006; Van Winckel et al. 2009; Bilíková et al. 2012; Clayton et al. 2014).

## 2. PLANET ENGULFMENT AS A TRIGGER FOR "DORMANT" SECULAR INSTABILITIES

### 2.1. *Planetary Systems as Suppressors of Secular Instabilities*

White dwarf pollution by tidally disrupted minor rocky bodies requires a mechanism to deliver asteroids from distant orbital separations into the stars's tidal disruption radius ($\sim 1R_\odot$). Nearly radial orbits may result from secular instabilities, which in some cases are capable of exciting eccentricities up to values of $\sim 1$. One well-known example of such instabilities is the KL mechanism (Kozai 1962; Lidov 1962; see Naoz 2016 for a recent review), which takes place when a distant stellar-mass companion is highly inclined respect to the orbit of the minor body. However, it is also known that additional bodies in the system may affect or entirely suppress the effect of the KL mechanism (e.g. Holman et al. 1997).

In the simplest scenario of one planet in a circular orbit with mass $M_{\rm p}$ and semi-major axis $a_{\rm p}$ inside a planetesimal's orbit ($a_{\rm p} < a$), the effect of the additional quadrupole potential due to the planet's time-averaged orbit will overcome that of the outer stellar companion if the planet-induced apsidal precession frequency

$$\dot{\varpi}_{\rm in} \simeq \frac{1}{2} n \left(\frac{M_{\rm p}}{M_{\rm s}}\right) \left(\frac{a_{\rm p}}{a}\right)^2 \approx n\epsilon_{\rm in}, \quad (1)$$

is larger than that induced by a binary with mass $M_{\rm b}$ and semi-major axis $a_{\rm b}$ of

$$\dot{\varpi}_{\rm out} \simeq n \left(\frac{M_{\rm b}}{M_{\rm s}}\right) \left(\frac{a}{a_{\rm b}}\right)^3 (1-e_{\rm b}^2)^{-3/2} = n\epsilon_{\rm out}, \quad (2)$$

with $n$ being the mean motion frequency of the planetesimal and where we have used the definition of two dimensionless quantities $\epsilon_{\rm in}$ and $\epsilon_{\rm out}$ that represent the relative strength of the tidal potentials (see the Appendix and Muñoz & Lai 2015).

When $\dot{\varpi}_{\rm in} = \dot{\varpi}_{\rm out}$, then $a = r_L$, where $r_L$ is the "Laplace radius", defined as

$$\begin{aligned} r_{\rm L} &\equiv \left(\frac{M_{\rm p}}{2M_{\rm b}} a_{\rm p}^2 a_{\rm b}^3 \left[1-e_{\rm b}^2\right]^{3/2}\right)^{1/5} \\ &\simeq 16.2 \text{ AU } \left(\frac{M_{\rm p}}{M_J}\right)^{1/5} \left(\frac{M_{\rm b}}{0.5M_\odot}\right)^{-1/5} \left(\frac{a_p}{2 \text{ AU}}\right)^{2/5} \\ &\quad \times \left(\frac{a_{\rm b}\sqrt{1-e_{\rm b}^2}}{600\sqrt{1-0.5^2} \text{ AU}}\right)^{3/5}. \end{aligned} \quad (3)$$

For $a < r_L$, the dynamics of the asteroid will be dominated by the planet's quadrupole potential, such that the planetesimal's angular momentum vector $\propto \mathbf{j}$ will precess around the planet's, with perfect alignment being the equilibrium solution. Conversely, for $a > r_L$, the dynamics of the asteroid will be dominated by the binary companion, with $\mathbf{j}$ precessing around the binary's angular momentum vector (with the possibility of being Kozai-unstable), with perfect alignment being the equilibrium solution. The smooth transition between these two regimes place takes rapidly around $a \simeq r_L$, and the general equilibrium solution of the equilibrium inclination $i_{\rm eq}$ for all values of $a$ is known as the "Laplace surface". For a test particle in a circular orbit, the

Laplace surface is given by (e.g., Tremaine et al. 2009; Tamayo et al. 2013):

$$\tan 2i_{\rm eq} = \frac{\sin 2i_{\rm b}}{\cos 2i_{\rm b} + 2(r_{\rm L}/a)^5} \quad (4)$$

where $i$ ($i_{\rm b}$) is the inclination of the test particle (binary) relative to the planetary system

Thus, for as long as there is a planet (or a planetary system) such that $r_L$ is large enough to accommodate a (nearly) coplanar population of planetesimals/asteriods, such bodies will be protected from the tidal potential from the binary companion, largely ignoring its presence throughout the main sequence (MS) evolution of the host star.

### 2.2. *Triggering of secular instabilities*

Any reduction of the quadrupole potential due to the planet will reduce the extent of the "safe zone" defined by the Laplace radius, progressively exposing bodies to the influence of the binary companion's tidal potential. One possible cause of such a change is planetary engulfment during the post main sequence stages of stellar evolution. During the red giant branch (RGB) and asymptotic giant branch (AGB) phases of the post-MS, low-to-intermediate mass stars can reach radii of a fraction of, or up to few AU, presumably engulfing all planets within this distance (Mustill & Villaver 2012; Villaver et al. 2014). In particular, the AGB phase is during which most of the mass in the stellar envelope is lost, resulting in the expansion of all the orbits in the system.

The engulfment of a planet consists of both its evaporation and its spiraling in during stellar expansion (potentially aided by the tidal interaction with the extended stellar envelope; Villaver et al. 2014). For simplicity, here we simply model the engulfment as the gradual reduction of the planetary semi-major axis $a_p$:

$$a_p(t) = a_{p,0} e^{-t/\tau_a} \quad \text{for} \;\; t_{\rm MS} < t < t_{\rm WD} \quad (5)$$

where $\tau_a$ represents the in-spiral timescale of the planet, $t_{\rm MS}$ is the duration of the stellar MS and $t_{\rm WD}$ is the time at which the WD is formed. As $r_L \propto a_{\rm p}^{2/5}$ (Eq. 3), planetary engulfment causes the Laplace radius the decrease.

In addition, we consider mass loss. If the expulsion of the stellar outer layers happens on timescales much longer than all the orbital periods in the system, then angular momentum conservation dictates that all semi-major axes evolve as $a/\dot{a} = -M_{\rm s}/\dot{M}_{\rm s}$ (e.g., Hadjidemetriou 1963; Veras et al. 2011). Thus, introducing another timescale $\tau_{\rm ml}$ we can write:

$$M_{\rm s}(t) = \begin{cases} M_{\rm s,0} e^{-t/\tau_{\rm ml}} & \text{if} \quad M_{\rm s,0} e^{-t/\tau_{\rm ml}} > M_{\rm WD} \\ M_{\rm WD} & \sim \end{cases} \quad (6)$$

for $t > t_{\rm MS}$. Which in turn implies $a(t) = a(0) e^{t/\tau_{\rm ml}}$ and $a_b(t) = a_b(0)(M_{\rm s,0} + M_{\rm b})/(M_{\rm s,0} e^{-t/\tau_{\rm ml}} + M_{\rm b})$ for $t_{\rm MS} < t < \tau_{\rm ml} \ln(M_{\rm s,0}/M_{\rm WD})$.

The effect of mass loss has an opposite effect to engulfment on the value of the Laplace radius ($r_L \propto a_b^{3/5}$). For $M_b \ll M_s$, one can write an approximate evolution of the Laplace radius:

$$\frac{r_{\rm L}(t)}{r_{\rm L}(0)} = \exp\Big[ -\frac{2t}{5\tau_{\rm a}} + \frac{3t}{5\tau_{\rm ml}} \Big], \; t_{\rm MS} < t < \tau_{\rm ml} \ln\left(\tfrac{M_{\rm s,0}}{M_{\rm WD}}\right) \quad (7)$$

which shows how mass loss and engulfment have opposite effects. Ultimately, engulfment is the determining factor, since $r_L, \to 0$ as $a_{\rm p} \to 0$, while mass loss stops when the stellar remnant mass reaches $M_{\rm WD}$[4].

The reduction of $r_L$ has a direct impact on the shape of the Laplace surface in Eq. (4). (1) If the "parameter" $r_L$ changes *very slowly*, the $i_{\rm eq}$ curve will evolve smoothly, and any bodies initially lying on the Laplace surface will remain on the final Laplace surface[5]. This implies full coplanarity with the binary companion when $r_L \to 0$, i.e., $i_{\rm final} \sim i_{\rm eq} \to i_{\rm b}$. (2) On the contrary, if $r_L$ is changed *very rapidly*, then the bodies initially lying on the Laplace surface will not be able to catch up, thus being frozen in their initial inclinations $i_{\rm final} \sim i_{\rm initial} \sim 0$. These two limits entail completely opposite consequences for the planetesimals: (1) if the planet is removed slowly, planetesimals will reach coplanarity with the companion, thus being Kozai-stable; (2) if the planet is removed suddenly, minor bodies will see their initial inclinations unchanged, thus being susceptible to KL oscillations.

#### 2.2.1. *Adiabaticity*

The speed at which $r_L$ is changed (either "very slow" or "very fast" as defined below) will determine whether configurations near equilibrium evolve "adiabatically" or not (e.g. Landau & Lifshitz 1969). Quantitatively, the rate of change in $\epsilon_{\rm in}$ (or in $r_L$) must be much smaller than the linear oscillation frequency $\omega_0$ around the equilibrium solution of the Laplace surface. Rewriting eq. (31) in Tremaine et al. (2009) as

$$\begin{aligned} \omega_0 = \frac{3}{2\sqrt{2}} n\epsilon_{\rm in} \Bigg[ & 1 + \cos 2i_{\rm eq} - \sin 2i_{\rm eq} \\ & + \frac{1}{2}\left(\frac{\epsilon_{\rm out}}{\epsilon_{\rm in}}\right)(\cos 2i_{\rm eq} + 2\cos 2i_{\rm b}) \\ & + \frac{1}{2}\left(\frac{\epsilon_{\rm out}}{\epsilon_{\rm in}}\right)^2 \cos^2 i_{\rm b} \Bigg]^{1/2} . \end{aligned} \quad (8)$$

The degree of adiabaticity can be represented by the ratio $|(\dot{r_L}/r_L)|/\omega_0$ (Landau & Lifshitz 1969), which is roughly

$$\frac{2}{3}\frac{\frac{2}{5}\tau_a^{-1}}{n\epsilon_{\rm in}} \sim \frac{1}{\dot{\varpi}_{\rm in}\tau_a} \;\; \text{if} \;\; \epsilon_{\rm out} \ll \epsilon_{\rm in} \;\; , \quad (9)$$

[4] Note that a planet is engulfed when it reaches the stellar envelope at $a_{\rm p} \simeq R_s$ at some point of the evolution (e.g., Mustill & Villaver 2012; Villaver et al. 2014), which is equivalent to setting $a_{\rm p} = 0$ in $r_{\rm L}$ because the quadrupole moment provided by the planet vanishes after engulfment (i.e., $\dot{\varpi}_{\rm in} = 0$ in Equation [1]).

[5] Note that a dynamical solution can "follow" a slowly changing fixed point *provided* this equilibrium remains stable. If the stability of the fixed point changes – i.e., it experiences a bifurcation – then adiabaticity is broken. The Laplace surface is known to become unstable in eccentricity (circular orbits are not allowed) in a narrow region of $a$ around $r_L$ only if $i_{\rm b} \gtrsim 69^\circ$ (Tremaine et al. 2009)

or

$$\frac{4}{3}\frac{\frac{2}{5}\tau_a^{-1}}{n\epsilon_{\rm out}\cos i_{\rm b}} \sim \frac{1}{\dot{\varpi}_{\rm out}\tau_a\cos i_{\rm b}} \sim \frac{\tau_{\rm KL}}{\tau_{\rm a}\cos i_{\rm b}} \text{ if } \epsilon_{\rm in} \ll \epsilon_{\rm out} \ , \tag{10}$$

where we have introduced the KL timescale (e.g., Antognini 2015)

$$\begin{aligned}\tau_{\rm KL} &= \frac{16}{15\pi}\left(\frac{a_{\rm b}\sqrt{1-e_{\rm b}^2}}{a}\right)^3\frac{M_{\rm s}}{M_{\rm b}}P \\ &\simeq 2.3\ {\rm Myr}\left(\frac{a}{10\ {\rm AU}}\right)^{-\frac{3}{2}}\left(\frac{a_{\rm b}}{600\ {\rm AU}}\right)^3(1-e_{\rm b}^2)^{3/2} \\ &\times\left(\frac{M_{\rm s}}{M_\odot}\right)^{\frac{1}{2}}\left(\frac{M_{\rm b}}{M_\odot}\right)^{-1}.\end{aligned} \tag{11}$$

Thus, after $r_L$ has shrunk below $a$, the two relevant timescales to compare will be $\tau_{\rm a}$ and $\tau_{\rm KL}$, and for evolution on the Laplace surface to be adiabatic, it is required that $\tau_{\rm a} \gg \tau_{\rm KL}$. As we will see below, this requirement will be rarely met by planet engulfment, and thus adiabaticity will be most commonly broken as $r_L \to 0$. For this reason, in most situations, planetesimals will be suddenly exposed to the KL mechanism once planet engulfment has been completed (see Fig. 1 for a schematic depiction). Thus, only after engulfment has removed the protection against eccentricity excitation, will the external perturber be enabled to place planetesimals into orbits leading to their disruption.

### 2.3. *Toy Model of Four Bodies with Octupole Terms*

In the absence of a planet, planetesimals will be susceptible to KL oscillations induced by the stellar binary provided that the relative inclination between the planetesimal and the binary $i_{\rm b}$ is in the range of $40^\circ - 140^\circ$. Nevertheless, for planetesimals with $a \sim 10$ AU to reach the tidal disruption distance of $\sim R_\odot$ at pericenter, their eccentricities must be such that $a(1-e) \sim R_\odot = 5\times10^{-3}$ AU, i.e $(1-e) \sim 10^{-3} - 10^{-4}$, which is difficult to achieve during quadrupole-order KL oscillations. The eccentric KL mechanism (Naoz 2016, which includes octupole-order terms in the tidal potential when $e_{\rm b} \neq 0$), on the other hand, is capable of producing such high eccentricities, thus satisfying the requirements for tidal disruption of planetesimals.

In order to study the evolution of planetesimals during the stellar MS and through the post-MS we integrated the (double-averaged) secular equations of a hierarchical four-body system (Hamers et al. 2015; Muñoz & Lai 2015) consisting of a star (of mass $M_{\rm s}$), a gas giant (of mass $M_{\rm p}$ and semi-major axis $a_{\rm p}$), a massless particle (semi-major axis $a$) and a distant companion (of mass $M_{\rm b}$ and semi-major axis $a_{\rm b}$). The initial setup is reminiscent of that of Muñoz & Lai (2015) but in this case we have included octupole-level terms in the potentials following Hamers et al. (2015) (see the Appendix of the current manuscript).

#### 2.3.1. *Equations of Motion*

We evolve the planetesimal's dimensionless specific angular momentum vector $\mathbf{j} = \sqrt{1-e^2}\ \hat{\mathbf{j}}$ and eccentricity vector $\mathbf{e}$ according to the equations of motion (e.g. Tremaine & Yavetz 2014):

$$\frac{d\mathbf{j}}{dt} = \frac{1}{\sqrt{\mathcal{G}M_{\rm in}a}}\Big(\mathbf{j}\times\nabla_{\mathbf{j}}\Phi + \mathbf{e}\times\nabla_{\mathbf{e}}\Phi\Big), \tag{12a}$$

$$\frac{d\mathbf{e}}{dt} = \frac{1}{\sqrt{\mathcal{G}M_{\rm in}a}}\Big(\mathbf{j}\times\nabla_{\mathbf{e}}\Phi + \mathbf{e}\times\nabla_{\mathbf{j}}\Phi\Big), \tag{12b}$$

where $M_{\rm in} = M_{\rm s}+M_{\rm p}$ and $\Phi = \Phi_{\rm in}+\Phi_{\rm out}$ is the combined tidal potential from the inner star-planet pair and the outer stellar companion including octupole-order terms (see Eqs [A1]-[A8]). The star-planet angular momentum and eccentricity vectors $\propto \mathbf{j}_{\rm in}$ and $\mathbf{e}_{\rm in}$ are evolved following an analogous set of equation of motion, except that the tidal potential is entirely due to the binary companion, with the contribution of the planetesimal being neglected. Finally, the angular momentum and eccentricity vectors of the star-binary system $\propto \mathbf{j}_{\rm out}$ and $\mathbf{e}_{\rm out}$ – although in principle subject to evolution under the tidal potential from the inner star-planet pair – are held constant and only the semimajor axis of this outermost orbit $a_{\rm out}$ is evolved consistently with the process of mass loss of the central star.

#### 2.3.2. *Initial set-up: main-sequence configuration*

We consider a host star with a Zero Age Main Sequence mass of $M_{\rm s} = 2M_\odot$, which is a typical progenitor for the currently-observed WD population in the Milky Way. We assume that this star is orbited by a Jupiter-mass planet at $a_{\rm p} = 2$ AU in a circular orbit, and a wide stellar binary companion with a mass of $M_{\rm b} = 0.5M_\odot$, a semi-major axis of $a_{\rm b} = 600$ AU and an eccentricity of $e_{\rm b} = 0.5$ (see panel a in Figure 1). The inclination relative to the planetary orbit is $i_{\rm b} = 80^\circ$. The planet is subject to the tidal field from the stellar companion and apsidal precession due to General Relativity (GR). At 2 AU, the apsidal precession period due to GR ($\sim 10$ Myr) is shorter than that due to the companion ($\sim 30$ Myr; Eq. [11]), and thus KL oscillations are suppressed. In practice, other sources of pericenter precession such as additional planets can make the planetary orbit long-term stable against perturbations from the inclined companion. In this configuration, $r_L \approx 16$ AU, and thus any bodies interior to this distance will be protected by the planet against perturbations from the binary companion. The fourth body in the system is a massless planetesimal located at $a = 10$ AU – such that $a < r_L$ – in near coplanarity with the planetary orbit ($i_{\rm eq} \simeq 0.46^\circ$ from Eq. [4])

#### 2.3.3. *Post-main sequence evolution*

The system is evolved at once (including MS and Post-MS stages, see the sequence depicted in Figure 1) under one set of equations (Eq. [12]). After some time $t_{\rm MS}$, mass loss and planetary engulfment are triggered (Eqs. [5] and [6]), affecting directly the semi-major axes $a_{\rm p}$, $a_{\rm b}$ and $a$ (which are constant in the secular evolution of the MS stage), in addition to the central mass $M_s$ (see Eqs. (A21)-(A23) in the Appendix). The timescale for planetary removal and mass loss is expected to be of a few Myr, and to take place primarily during the AGB phase of stellar evolution (e.g., Hurley et al. 2000). We set $\tau_{\rm ml} = 4\tau_a$ to ensure that the mass loss and the orbit's

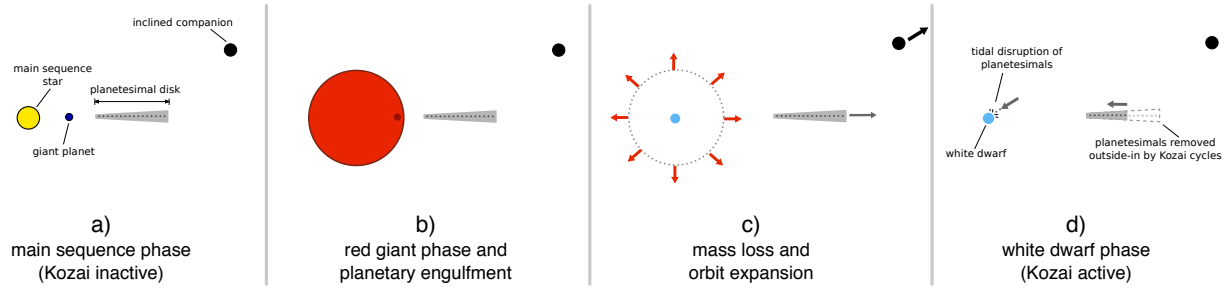


FIG. 1.— The orbital architectures at the different phases of the stellar evolution considered in our example. *Panel a*: a $2M_\odot$ MS star orbited by a giant planet at $a_{\rm p} = 2$ AU, a coplanar planetesimal disk at $a = 3-12$ AU, and inclined binary companion ($i_{\rm b} = 80°$) at $a_{\rm b} = 600$ AU. The disk remains stable against the KL mechanism because of the planet perturbations. *Panel b*: the planet is engulfed by the host star during the giant phase (GB or AGB phases). *Panel c*: the orbits of the planetesimal disk and the binary expand due to mass loss. *Panel d*: the disk is subject to the KL mechanism and the planetesimals are tidally disrupted outside-in.

shrinkage happen simultaneously, but the former takes place mostly at the end of the planet's orbital decay. During this phase, planets inside $\sim 3-5$ AU are expected to be engulfed by the expanded envelope of the host star (Mustill & Villaver 2012; Villaver et al. 2014). By using the secular equations of motion it is implicitly assumed that the mass loss and engulfment timescales are much longer than all the orbital timescales in the system. For outer companion separations of up to $\sim 2000$ AU, this is a reasonable approximation. In such case, all the orbital elements in the system, except the semi-major axes, will remain unchanged (e.g., Hadjidemetriou 1963; Veras et al. 2011).

In our example, we use that the final mass – the mass of the WD – is $M_{\rm WD} \simeq 0.64 M_\odot$ (Hurley et al. 2000). The semi-major axes of the small bodies expands in factor of $M_{\rm s}(t=0)/M_{\rm WD} \simeq 3.1$, while the binary does so in a factor of $[M_{\rm s}(t=0)+M_{\rm b}]/(M_{\rm WD}+M_{\rm b}) \simeq 2.2$. Initially, $\epsilon_{\rm in}/\epsilon_{\rm out} = (r_{L,0}/a)^5 \approx 11$. As the planet is engulfed, $\epsilon_{\rm in}/\epsilon_{\rm out} \to 0$; in practice, the potential from the planet is ignored after $\epsilon_{\rm in}/\epsilon_{\rm out}$ reaches $10^{-5}$, or when $r_L = 0.1a$.

After the planet influence becomes negligible, the planetesimals pericenter precession will be given by $\dot{\varpi}_{\rm out}$ (Eq. 2). If the removal of the planet is non-adiabatic (as defined in Section 2.2.1), the planetesimal may be subject to KL oscillations, which take place with a characteristic period of $\tau_{\rm KL} \sim \dot{\varpi}_{\rm out}^{-1}$. In classic Kozai oscillations (quadrupole-order perturbations $\propto a^2/a_{\rm b}^3$) the planetesimals eccentricity may reach $e_{\rm max} = (1 - 5/3\cos^2 i_{\rm b})^{1/2} \simeq 0.97$, implying a minimum pericenter distance of $a(1-e_{\rm max}) \simeq 1$ AU. However, for $e_{\rm b} \neq 0$, the planetesimal is subject to strong forcing due to higher-order (mostly octupole-order $\propto e_{\rm b} a^3/a_{\rm b}^4$) perturbations, which happen in timescales longer than the KL timescale (e.g. Naoz 2016). These *very long timescale* effects can drive the eccentricity up to much higher values ($1-e \lesssim 0.001$). If high enough eccentricities are reached such that $a(1-e) < 2R_\odot$, then the planetesimal is assumed to be tidally disrupted.

### 2.3.4. *Fast and slow planet engulfment*

To directly test the qualitative predictions of Section 2.2, we integrate the 4-body equations of motion while varying the engulfment time $\tau_{\rm a}$. As described in Section 2.2.1, the ratio $\tau_{\rm a}/\tau_{\rm KL}$ will determine whether or not the planetesimal will be susceptible to the influence of the eccentric KL mechanism.

*Fast engulfment ($\tau_{\rm a} = 0.5$ Myr)*— For $\tau_{\rm a} \ll \tau_{\rm KL} \sim 8$ Myr (left panels, Fig. 2), we expect adiabaticity to be broken and the planetesimal to be impulsively removed from the Laplace surface. In this case, orbits expand according to the mass loss prescription (top panel), but this takes place before the planetesimal inclination has been altered significantly (bottom panel). The planetesimal-to-binary inclination is this the same as in the initial condition ($\sim 80°$), which is capable of triggering KL oscillations. After planet removal, common KL oscillations ensue (with period of $\simeq 10$ Myr), reaching a maximum planetesimal eccentricity of 0.9. In the longer run, the slower octupole-level oscillations cause dramatic eccentricity growth, reaching $e \simeq 0.999$ and beyond, sufficient to guarantee tidal disruption.

*Trans-adiabatic engulfment ($\tau_{\rm a} = 10$ Myr)*— When $\tau_{\rm a} \sim \tau_{\rm KL}$ (Fig. 2, middle panels), the orbital behavior of the planet is markedly different from the "fast engulfment" case from above. In this case, the planetesimal "tries to follow" the Laplace surface solution $i_{\rm eq}(r_L)$ (Eq. [4]) as $r_L$ shrinks with time. Initially, the planetesimal can follow closely; the initial oscillation amplitude ($\lesssim 2°$) is seeded by the imperfect alignment of $i_0$ with $i_{\rm eq}$ at $t = 0$. If adiabaticity were to be preserved, this initial amplitude should grow as the oscillation frequency decreases from $\sim \dot{\varpi}_{\rm in}|_{t=0}$ to $\sim \dot{\varpi}_{\rm out}$[6]. Nevertheless, planet engulfment is still too fast, as the planetesimal leaves the Laplace surface before the planet is fully engulfed. In this case, the planetesimal is decoupled from the planet at $t \simeq 20$ Myr (the planet is finally eliminated at $t \simeq 30$ Myr), with an inclination relative to the binary of $\gtrsim 40°$. This small inclination ($> 39.23°$) is still large enough to trigger some mild KL oscillations, but evidently it is far from the inclinations needed to obtain tidal disruptions as $e_{\rm max}$ is only $\simeq 0.45$.

*Slow engulfment ($\tau_{\rm a} = 100$ Myr)*— For slow engulfment ($\tau_{\rm a} \gg \tau_{\rm KL}$, right panels, Fig. 2), the planetesimal nearly follows the Laplace surface to the end of the integration, reaching a final inclination of only $\sim 13°$ and a finite constant eccentricity of $\simeq 0.3$. The finite eccentricity is reached at $\simeq 60$ Myr when $a \sim r_L$, and is due to the bifurcation experienced in the Laplace equi-

[6] Linear oscillations around the stable equilibrium should behave like a harmonic oscillator of time-varying frequency $\omega_0(t)$ (Eq. 8), for which the action is $E/\omega_0 = \omega_0 A^2/2$, where $A$ is the oscillation amplitude. For very slowly varying $\omega_0$, the action $E/\omega_0$ is an adiabatic invariant.

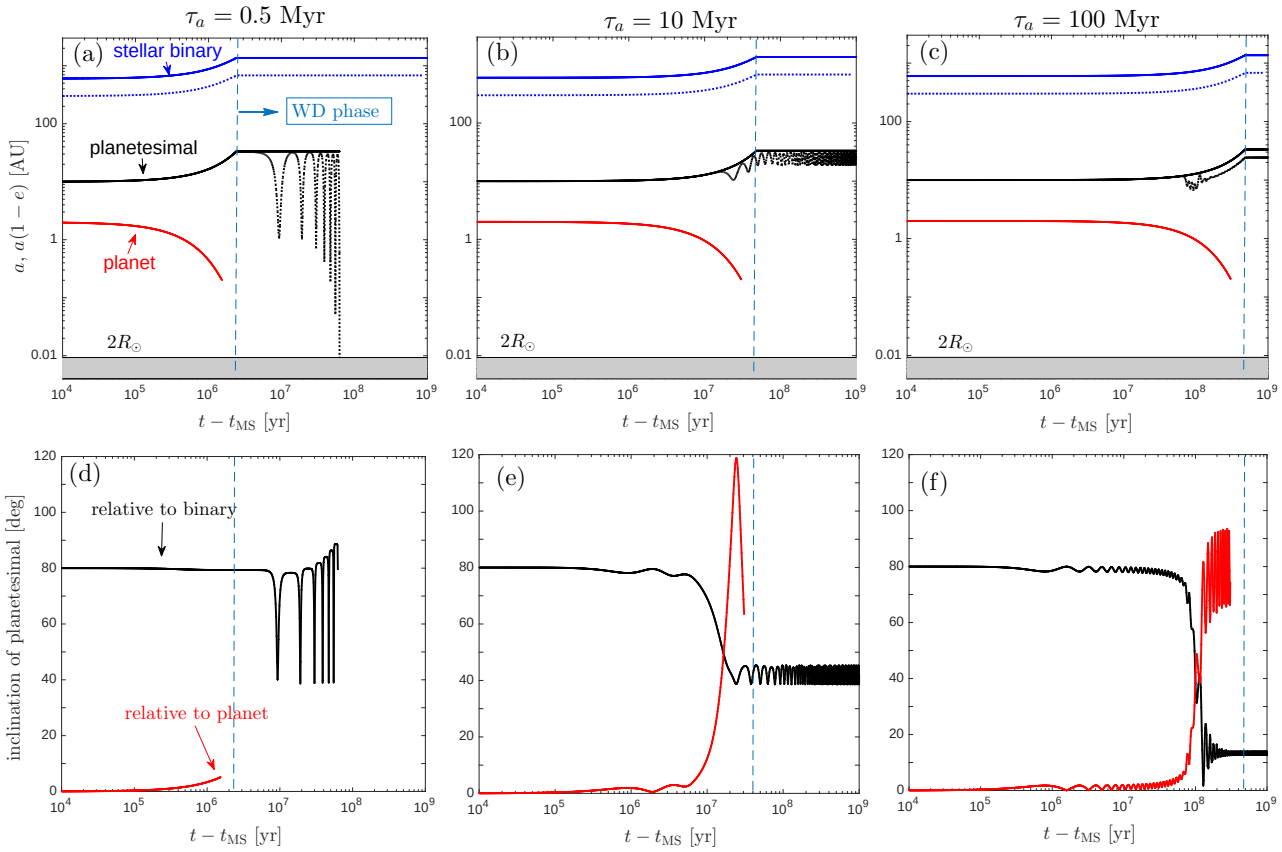


FIG. 2.— Orbital evolution of the planetary system initially composed of an inner Jupiter-mass planet at 2 AU and a massless planetesimal at 10 AU orbiting a $2M_\odot$ star (final WD mass of 0.64 $M_\odot$). We show the results after the main sequence ($t > t_{\rm MS}$) and the vertical dashed lines indicate the zero WD's cooling age. The planetesimal and the planets start with zero mutual inclination and circular orbits, while the binary companion with $M_b = 0.5M_\odot$ and $a_b = 600$ AU has an inclination of 80° relative to the planetary system. The eccentricity of the binary is $e_b = 0.5$, and the initial ascending nodes and arguments of pericenter are 0 for all the orbits. The upper panels (a, b, and c) show the semi-major axes (solid lines) and pericenter distances (dotted lines). The lower panels (d, e, and f) show the inclination of the planetesimal relative to the planets (solid red line) and relative to the binary (solid black line). The different columns show the different planet's semi-major axes decaying timescale $\tau_a$ in Equation (5): $\tau_a = 0.5$ Myr (panels a and d), $\tau_a = 10$ Myr (panels b and e), and $\tau_a = 100$ Myr (panels c and f). The planet is assumed to be engulfed at 0.2 AU and the planetesimal is assumed to be tidally disrupted when it reaches $a(1-e) < 2R_\odot$, which only happens for $\tau_a = 0.5$ Myr (dotted black line in panel a). We set the mass loss timescale $\tau_{\rm ml} = M_s/|\dot{M}_s|$ equal to $4\tau_a$ to ensure that mass is lost most efficiently after the planet is engulfed.

librium solution, which makes circular orbits unstable (Tremaine et al. 2009; Tamayo et al. 2013). For even slower engulfment ($\tau_{\rm a} = 1$ Gyr), the final state is much more steady, i.e., inclination oscillations are small, and the planetesimal never leaves the vicinity of the Laplace surface, even if it gains a finite eccentricity as it crosses the bifurcation. We note that this bifurcation exists only when the planet-binary inclination is $\gtrsim 69°$. In addition, the finite octupole potential from the binary introduces modifications to the classical Laplace equilibrium analysis (e.g. Muñoz & Lai 2015). In an analogous example with $e_{\rm b} = 0$ and a lower inclination we obtain an end-state where the planetesimal is in perfect alignment with the binary and retains zero eccentricity throughout the integration.

Of these three scenarios, only the first one (fast engulfment) is expected to resemble the AGB phase, which lasts less than $\sim 10$ Myr. This introduces an important difference with the work of Muñoz & Lai (2015), which finds that the rate of reduction of $r_L$ is always slower than the oscillations around the equilibrium solution. In the present case, adiabaticity is an unlikely outcome, which implies that planetesimals can "instantaneously" see themselves in a Kozai-unstable configurations even though throughout the entire MS lifetime of the host star they were protected against such instabilities.

Finally, we caution that our numerical calculations are based on the double orbit averaging approximation and might not represent the dynamics properly, leading to spurious extreme eccentricities required to disrupt the planetesimal (Luo et al. 2016). To this extent, we have repeated the three-body integrations after planet engulfment using the direct high-order N-body integrator IAS15 (Rein & Spiegel 2015), which is part of the REBOUND package (Rein & Liu 2012). We find that the evolution looks very similar, but the planetesimal is disrupted slightly later after two extra oscillation cycles compared with the secular code.

## 3. EVOLUTION OF THE PLANETESIMAL DISK

We integrate the orbital evolution of a disk of collisionless planetesimals orbiting a white dwarf and perturbed by a distant companion based on the orbital configura-

tion of our fiducial system described in §2.2. This phase corresponds to panel d in Figure 1.

### 3.1. *Initial conditions*

After the AGB phase we are left with a a WD of mass $M_{\rm WD} \simeq 0.64 M_\odot$ orbited by a planetesimal disk and stellar binary companion with mass of $M_{\rm b} = 0.5 M_\odot$, semi-major axis $a_{\rm b} = 1300$ AU, and inclination of $i_{\rm b} = 80^\circ$ (relative to the planetary orbit before engulfment).

We shall assume that the planetesimal disk has the following power-law profile for the surface density

$$\Sigma(a) = \frac{M_{\rm disk}}{2\pi\left(a_{\rm out} - a_{\rm in}\right)} \cdot \frac{1}{a}, \tag{13}$$

where $M_{\rm disk}$ is the total mass of the disk, while $a_{\rm in}$ and $a_{\rm out}$ are its inner and outer boundaries. This power-law profile has a uniform mass distribution as a function of semi-major axis, which is a convenient choice to easily read out our results for the accretion rates.

The inner edge of the disk $a_{\rm in}$ is set by the dynamical stability due to the planetary perturbations during the Main Sequence. Since the planet is initially at $a_{\rm p} = 2$ AU, the long-term stability is guaranteed for planetesimals at $\gtrsim 3$ AU[7]. Since the semi-major axis of the planetesimals expands by a factor of $\simeq 3.1$ relative to the initial value during the MS, we set $a_{\rm in} = 10$ AU.

The outer edge is set by the location of the Laplace radius, beyond which the secular perturbations due to the binary can excite the eccentricities and inclinations of the planetesimals. More specifically, as shown by Tremaine et al. (2009) for a binary's inclination of $i_{\rm b} = 80^\circ$ a test particle is stable against eccentricity perturbations when $a < 0.9 r_{\rm L} \simeq 14.6$ AU. Thus, we conservatively consider the planetesimals with $a < 12$ AU in our calculations so the disk remains nearly aligned with the orbit of the planet and with low-eccentricity excitation during the planet engulfment. For reference, the Laplace surface of a planetesimal with $a = 12$ AU has an inclination relative to the planetary orbit of $i_{\rm eq} \sim 1.1^\circ$ (Eqs. [4] and [3]). Again, since the semi-major axis of the planetesimals expands by a factor of $\simeq 3.1$ relative to the initial value during the MS, we set $a_{\rm out} = 35$ AU.

The planetesimal orbits are initialized with zero inclination, random longitudes of the ascending node and arguments of pericenter, and eccentricities from a Rayleigh distribution with parameter 0.01.

We leave the mass of the disk as a free parameter, but keep in mind that the collisional evolution of the disk limits the maximum mass for a given age (e.g., Wyatt et al. 2007; Heng & Tremaine 2010). We discuss the constraints on the disk mass in §4.

### 3.2. *Results*

We evolve the disk up to 10 Gyr using $50,000$ particles and record the time at which a particle is tidally disrupted, which we define to takes place once $a(1-e) < 2R_\odot$. The results are not sensitive to the choice of the disruption distance, and typical values within $\sim 1-3R_\odot$ (Veras et al. 2014) give similar results.

[7] The test particles are Hill stable for $a/a_p \gtrsim 1.4$ (e.g., Gladman 1993).

In Figure 3 we show the number of disrupted bodies as function of the initial semi-major axes and the disruption times. From panel a we observe that the bodies at larger semi-major axes tend to be disrupted first. This is expected because the KL timescale decreases with semi-major axes as $a^{-3/2}$ (see Equation 11). However, we point out from panel a that for a given semi-major axis the disruptions happen at many different times, not just $\tau_{\rm KL}$. This is because the binary is eccentric ($e_{\rm b} = 0.5$) and we expect the dynamics of the disk to be affected by the octupole-level eccentricity modulations of the KL mechanism[8](see Naoz 2016 for a recent review), which lead to extreme eccentricities on timescales longer than $\tau_{\rm KL}$.

The strength of these octupole-level perturbations (relative to the quadrupole-level) is proportional to $\epsilon_{\rm oct} = e_{\rm b} a/a_{\rm b}$, which implies that the planetesimals with smaller semi-major axes are expected to be less affected by the octupole modulations. Consistently, we observe from panels a and b that the number of disruptions decreases from $\gtrsim 90\%$ at $a \lesssim 20$ AU to nearly zero for $a \lesssim 14$ AU. Overall, 70% of the planetesimals are tidally disrupted (see panel b of Figure 3) .

Similarly, the timescale is of these octupole-level oscillations is $\sim \epsilon_{\rm oct}^{-1/2} \tau_{\rm KL} \propto a^{-2}$ (Antognini 2015). Therefore, the small bodies are disrupted after several secular timescales $\tau_{\rm KL}$ giving rise to a wide range disruptions times for a fixed semi-major axis. From panel c we observe that the disruption times have a wide distribution in the range of $\sim 0.05 - 10$ Gyr. The distribution peaks at $\sim 0.1$ Gyr because the first modulation of the octupole is driving most of the planetesimals to extremely large eccentricities around this time.

Beyond this peak, the distribution flattens in log of the time, $dN/d\log(t) \sim$ cst., meaning that it decays as $\propto 1/t$ at late times. This slow decay is due to extra octupole-level modulations of the planetesimals that survived the first one high eccentricity phase, which happens preferentially for smaller values of $a$, as expected.

In summary, most of the planetesimal disk ($\sim 70\%$ of the mass) is tidally disrupted in a wide range of timescales due to both the long-term octupole-level perturbations and the large radial extent of the disk. The rate of disruption events decays slowly as $\propto 1/t$ at late times.

## 4. DISCUSSION

We have proposed a new mechanism to explain the observed pollution in WDs through the tidal disruption of planetesimals orbiting these stars. We propose that a planetary system (one or several planets inside $\sim 2-5$ AU) shield the planetesimals orbits against the KL mechanism due a distant stellar companion. Once the planetary system is engulfed during the late stages of stellar evolution (e.g., the AGB phase), the orbits of the planetesimals become (secularly) unstable, leading to extreme eccentricities ($e \gtrsim 0.999$) and, therefore, to tidal disruptions.

This mechanism has the following properties:

[8] Note that the maximum eccentricity with $e_{\rm b} = 0$ is $e_{\rm max} = (1 - 5/3\cos^2 i_{\rm b})^{1/2} = 0.975$, which it does not lead to disruptions since $a(1-e_{\rm max}) > 0.3$ AU.

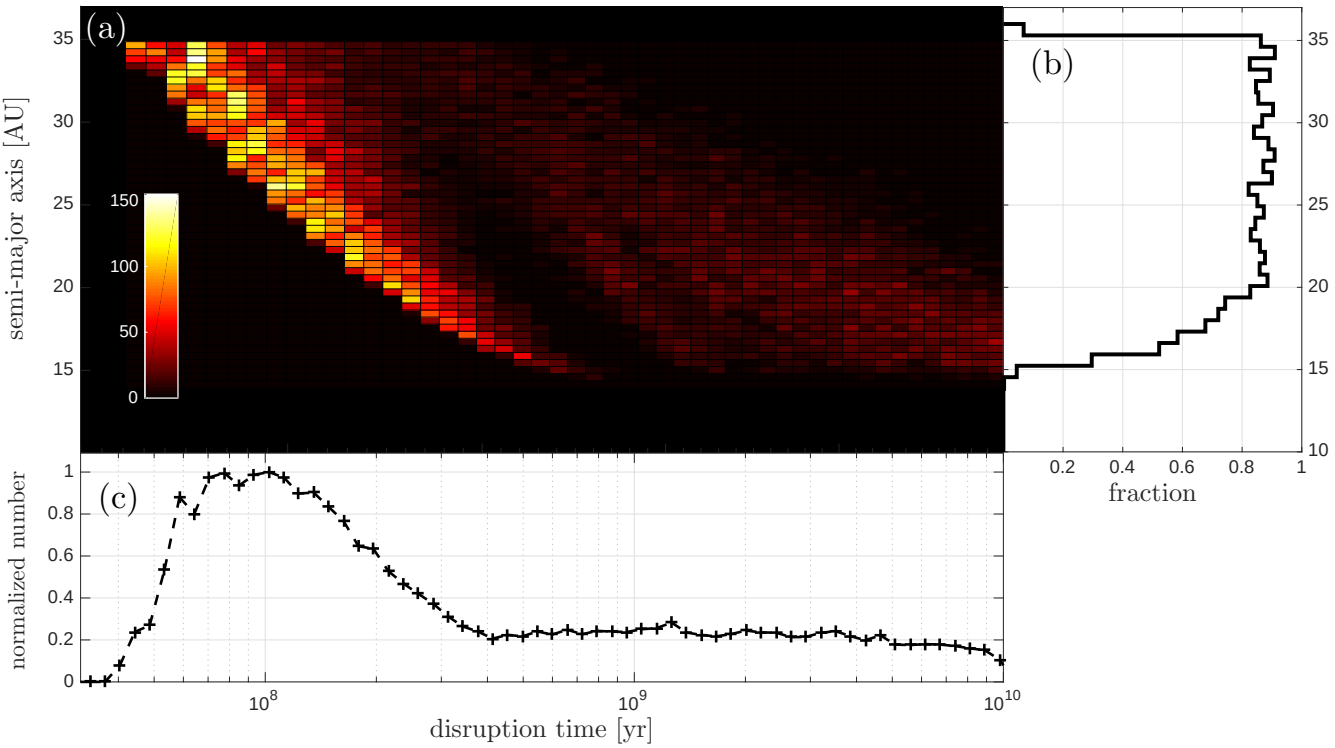


FIG. 3.— Number of particles that are tidally disrupted by the WD as a function of their initial semi-major axis during the WD phase (i.e., after their orbits expanded by a factor of $\simeq 3.1$ relative to their MS values) and the time at which they cross the disruption distance (initial time is the zero cooling age time). *Panel a:* two-dimensional histogram. The binning in the horizontal axis is evenly-spaced in the log of the disruption time. *Panel b:* fraction of tidally disrupted particles as a function of semi-major axis. *Panel c:* number of tidally disrupted particles normalized by the tallest bin as a function of the disruption time.

1. *pollution takes place for WDs of all cooling ages.* This property, required by the observational evidence, is inherent to the nature of the eccentric KL mechanism, which leads to the excitation into extreme eccentricities over very long timescales.

2. *It provides a steady flux of tidally disrupted rocky bodies.* This property is due the large radial extent of the planetesimal disk, widely spanning different disruption timescales. Each part of the disk has a disruption timescale $\propto a^{-2}$ (the eccentric KL timescale). Furthermore, disruptions can happen after multiple eccentric KL cycles. This property is required in order to have a non-negligible probability of observing the metals in the WDs atmosphere, since both the accretion and settling timescales are much shorter than the cooling ages of the observed systems. We quantify this probability in §4.3 (see Equation [17]).

3. *The planetesimal disk can have low surface densities and be long-lived.* Since the planetesimal disk can have a large radial extent ($\Delta a/a \sim 3.5$ in our example in Figure 3) and most of the disk can disrupted ($\sim 0.7$ of the mass), our mechanism can explain the observed accretion rates even for low surface densities (see constraints in §4.2). These low surface density disks can live for longer timescales avoiding grinding down to dust, which would be easily blown out during the RG and AGB phases by radiation pressure (e.g., Bonsor & Wyatt 2010).

Regarding point 1 above, we note that a similar idea, relying on long-timescale secular instabilities to explain the pollution of the oldest WDs have been presented by Bonsor & Veras (2015) and Hamers & Portegies Zwart (2016). These models, however, have not yet shown to provide the required steady flux of disrupting rocky bodies (point 2 above), nor consider the shielding effect against external perturbations that planetary systems would have during the MS phase of the host star.

In what follows, we discuss further constraints on our model from both observations and theoretical expectations.

### 4.1. *Constraints on the disk mass $M_{\rm disk}$*

Disks with high enough masses can quench our mechanism by (at least) the following two reasons: (1) pericenter precession rate due to self-gravity limits the KL mechanism; (2) dynamically hot disks become highly collisional, likely shattering the small bodies.

The pericenter precession timescale of a planetesimal at 10 AU (the inner edge of our disk) due to the self-gravity of the disk has been estimated by Batygin et al. (2011) to be (see also Rafikov 2013; Tamayo et al. 2015):

$$\tau_{\rm s-g} \sim 13 \text{ Myr} \left(\frac{M_\oplus}{M_{\rm disk}}\right). \quad (14)$$

This timescale should be compared to the timescale of pericenter precession due to the external companion, $\tau_{\rm KL}$ (Equation 11). For the example with $a_{\rm b} = 1300$ AU and $a \sim 10-35$ AU, $\tau_{\rm KL} \sim 4-24$ Myr, implying that, for the KL mechanism to operate, we require $M_{\rm disk} \lesssim 0.5 M_\oplus$. However, when $\tau_{\rm s-g} \gtrsim \tau_{\rm KL}$, the maximum eccentric-

ity reached by the KL mechanism is still reduced (e.g. Liu et al. 2015) and thus the planetesimals do not reach star-grazing orbits. We checked the effect of disk self-gravity by adding a pericenter precession term to equations of motion with a rate $\sim 1/\tau_{\rm s-g}$, finding that a range of maximum disk masses in $\sim 0.01 - 0.1 M_\oplus$ still allows for numerous tidal disruptions.

After KL oscillations stir up the planetesimal disk, the relative velocities between the planetesimals are high ($e \sim i \sim 1$), and the collisions between planetesimals can be highly disruptive. Heng & Tremaine (2010) have estimated that a dynamically hot planetesimal disk at $\sim$ 10 AU can survive the disruptive collisions or the gravitational scattering events for Gyr timescales if $M_{\rm disk} \lesssim M_\oplus$. However, such disks should be comprised of $\lesssim 10^4$ small bodies, each with at least a Ceres mass of $\sim 10^{24}$g $\sim 10^{-4}$M$_\oplus$. These constraints relax dramatically for disks at larger semi-major axes. For example, at 100 AU, the disk can be as massive 100 $M_\oplus$ and allow for body numbers of up to $10^{10}$ and individual masses of $10^{19}$ g. In our model, a disk with radial extent of $\sim 10 - 40$ AU and a mass of $M_{\rm disk} \lesssim M_\oplus$ should survive in the long term.

In conclusion, our mechanism is expected to operate in disks with masses of $\lesssim 0.1 M_\oplus$. Higher masses are expected to either quench the KL oscillations or disrupt the disk via collisions between the planetesimals.

### 4.2. *Accretion rates*

Having constrained the initial mass of the disk to $M_{\rm disk} \lesssim 0.1 M_\oplus$, we can estimate the maximum accretion rate of planetesimals predicted by our model as a function of age. For simplicity, we shall assume that the size distribution of the planetesimals does not change with semi-major axes.

The total mass accreted by the WD can estimated as:

$$M_{\rm acc} = f_{\rm td} \cdot f_{\rm acc} \cdot M_{\rm disk} \tag{15}$$

where $f_{\rm td}$ is the fraction of tidally disrupted objects and $f_{\rm acc}$ is the mass fraction of disrupted particles that is accreted and reaches the WD's surface. We estimate the former fraction directly from our simulation (see panel b of Figure 3) to be $f_{\rm td} \simeq 0.7$. The latter fraction is largely unconstrained.

The accretion rate can be calculated as

$$\frac{dM_{\rm acc}}{dt} = \frac{df_{\rm td}}{dt} \cdot f_{\rm acc} \cdot M_{\rm disk}, \tag{16}$$

where $df_{\rm td}/dt$ is shown in panel c of Figure 3 (normalized by the maximum rate). From this figure we point out that the frequency of disrupted bodies and, therefore the accretion rate, is highest at $\sim 50-300$ Myr and it flattens (in log space, i.e., decays as $\propto 1/t$) at $\gtrsim 500$ Myr.

In Figure 4, we show the accretion rate derived from our calculations by computing the time between tidal disruptions and assuming that all the bodies have the same mass. We set $f_{\rm acc} = 1$ and quote values of the disk mass $M_{\rm disk}$.

In panel a, we show the accretion rate for different disk masses in a range of $M_{\rm disk} = 10^{-5} - 10^{-1} M_\oplus$, where the upper limit is roughly the maximum mass imposed by precession due to disk self-gravity (see §4.1). The distribution of accretion for $M_{\rm disk} = 0.1 M_\oplus$ (solid black line) peaks at $\sim 3 \times 10^{10}$ g s$^{-1}$, while there is a secondary bump at $\sim 10^9$ g s$^{-1}$. This bi-modality is due to the accretion rate change at early and late times in the evolution of the WD (see panel c of Figure 3). By splitting the sample into early stages (cooling ages $<$ 500 Myr) and late stages (cooling ages $>$ 500 Myr), we obtain two symmetric (log-normal) distributions. For reference, we show a fit to the observations using a log-normal distribution with $\mu = 8$ and $\sigma = 1.3$ taken from Wyatt et al. (2014). In panel b, we show the accretion rates at early and late stages for disk masses of $M_{\rm disk} = 2.5 \times 10^{-4} M_\oplus$ and $M_{\rm disk} = 0.01 M_\oplus$, both coinciding with the observed peak at $10^8$ g s$^{-1}$.

We also note from the panel b that our model predicts a smaller dispersion of the accretion rates relative to the observations. In reality, we expect that for an ensemble of systems our predicted accretion rates should broaden significantly by considering a distribution of disk masses and particle masses, as well different orbital separations of the binary companion. This calculation is beyond the scope of this paper and it will be worth studying in a future work.

In summary, we find that disk masses in the range $M_{\rm disk} = 10^{-4} - 10^{-2} M_\oplus$ produce accretion rates consistent with observations. These disk masses are small enough that this mechanism is not expected to be limited by either by disk self-gravity or the collisional destruction of small bodies (see §4.1). The accretion rate is expected to peak at $\sim 10^8$ yr and decays as $\propto 1/t$ at late times.

### 4.3. *Estimate of the pollution rate*

Here we estimate the rate at which this mechanism might contribute to the observed pollution of WDs and assess whether it can account the high observed rates of $\sim 25 - 50\%$.

The fraction of WDs for which our mechanism can contribute to the observed levels of pollution can be estimated as:

$$f_{\rm poll} \equiv f_T \cdot f_{\rm KL} \cdot f_b \cdot f_p, \tag{17}$$

where $f_T$ is the fractional time in the WD's cooling age during which the rocky material is being supplied, $f_{\rm KL}$ is the fraction of systems that leading to planetesimal disruptions due to the eccentric KL mechanism, $f_b$ is the fraction of stars with wide ($a_b > 100$ AU) binary companions, and $f_p$ is the fraction of planetary systems with planets within $\sim 3$ AU and planetesimal disks during the main sequence of A and F stars.

We can optimistically estimate that $f_T \sim 1$ since the proposed system provides a steady delivery of asteroids into disrupting orbits (see panel c in Figure 3). In reality, we have to account for the finite number of planetesimals in the system which would lead to discontinuous events of tidal disruptions. However, this effect is compensated by the finite timescales involved in the circularization of the disrupted material and subsequent accretion onto the WD's atmosphere (see Veras 2016). We emphasize that one of the virtues of this new mechanism is that $f_T \sim 1$, which is not the case in many others models found in the literature.

The fraction of systems for which the planetesimals can be tidally disrupted due the eccentric KL mechanism

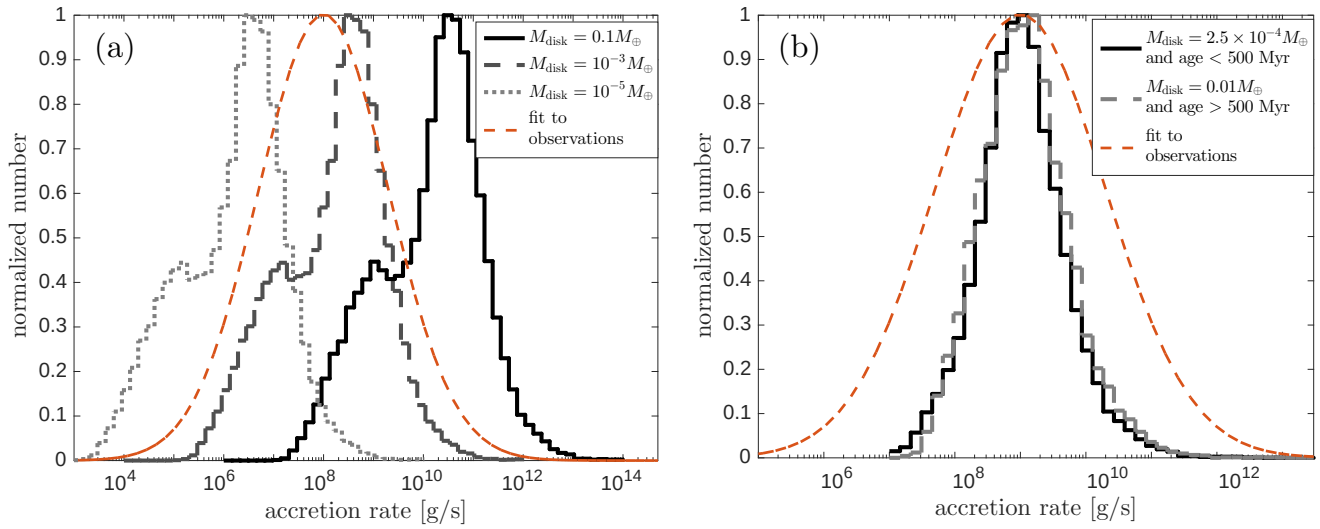


FIG. 4.— Accretion rates derived from the number of small bodies disrupted in our model in Figure 3 for different disk masses $M_{\rm disk}$ and cooling ages. We assume that all the particles have the same mass and that $f_{\rm acc} = 1$ in Equation (15), i.e., all the mass in tidally disrupted particles is accreted by the WD. *Panel a:* we set $M_{\rm disk} = 0.1 M_\oplus$ (solid black line), which is the largest mass allowed by the precession due to the self-gravity of the disk, and also show lower values of $M_{\rm disk} = 10^{-3} M_\oplus$ (dark gray dashed line) and $M_{\rm disk} = 10^{-5} M_\oplus$ (light grey dotted line). A fit to the observations taken from Wyatt et al. (2014) is shown in red dashed line. *Panel b:* we divide the accretion rates in panel a in two different populations: cooling ages $< 500$ Myr with $M_{\rm disk} = 2.4 \times 10^{-4} M_\oplus$ (solid black line) and cooling ages $> 500$ Myr $M_{\rm disk} = 0.01 M_\oplus$ (gray dashed line). The disk masses in each population are set to reproduce the observed peak in the observations (red dashed line).

$f_{\rm KL}$ can be estimated from previous studies in the context of planet disruptions in main sequence stars (e.g., Naoz et al. 2012; Petrovich 2015a; Anderson et al. 2016; Muñoz et al. 2016). These studies find that for a population of wide binaries ($a_{\rm b} \gtrsim 100$ AU) with isotropic inclinations and a thermal eccentricity distribution[9] roughly up to $\sim 30\%$ of them can lead to planetary tidal disruptions (assuming no tidal circularization). This estimate is consistent with the observation that $5/17 \sim 30\%$ of the WDs with wide binary companions are metal-polluted (Zuckerman 2014). Thus, $f_{\rm KL} \simeq 0.3$.

The fraction of A and F stars (progenitors of most WDs) with binary companions has been measured to be $\sim 70\%$ (Kouwenhoven et al. 2007; Peter et al. 2012; De Rosa et al. 2014), while the semi-major axis distribution follows a log-normal distribution peaked at $\sim 300$ AU (De Rosa et al. 2014), which is significantly wider than the peak of Solar-type stars at $\sim 40$ AU (Raghavan et al. 2010). Using the semi-major axis distribution from De Rosa et al. (2014), we find that $\sim 70\%$ of the binaries have $a_{\rm b} > 100$ AU, implying that the fraction of A stars with wide binary companions is $\sim 0.7 \times 0.7 \sim 0.5$. Thus, we estimate that the fraction of A stars with wide binary companions is $f_b \sim 0.5$.

The fraction of A and F stars with planetary systems and outer small rocky bodies $f_p$ can be estimated –conservatively– from the occurrence of gas giant planets (assuming they all have small rocky bodies). The RV planet searches find that $\gtrsim 10\%$ of Solar-type stars have gas giant planets (e.g., Winn & Fabrycky 2015), while the occurrence seems increase linearly with the host star mass, reaching $\sim 30\% \pm 15\%$ for A-stars with $2 M_\odot$ stars (Johnson et al. 2010). Lower-mass planets around Solar-type stars are more abundant than giants, and their occurrence, which is not well constrained at AU separations and for A and F stars, is roughly 0.5. The extrapolation of these results suggest that the occurrence of planets in A and F stars can be as high unity. Thus, we use $f_p \sim 0.3 - 1$.

Putting these numbers together, we estimate that the fraction of polluted WDs that can be explained by our mechanism is $f_{\rm poll} = f_T \cdot f_{\rm KL} \cdot f_b \cdot f_p \sim 1 \times 0.3 \times 0.5 \times (0.3 - 1) \sim 0.05 - 0.15$. This result implies that our mechanism can explain a significant portion, but not all, of the observed polluted WDs, which amount to fraction of $f_{\rm poll,obs} \gtrsim 0.25$.

In summary, our mechanism can only explain a fraction, although still significant (up to 50%), of the observed polluted WDs. Complete searches for companions, for which GAIA will play a crucial role, might shed light on the significance of this new model to explain the pollution of WDs.

### 4.4. *Outer companions in polluted white dwarfs*

The engulfment-aided KL mechanism to explain WD pollution requires the presence of a massive body in a wide orbit (either a stellar companion or a planet). We note that both the distance and the mass of the distant perturber enter into the calculation mainly through the timescale of the gravitational perturbations in the form of the dimensionless parameter $\epsilon_{\rm out} \propto M_{\rm out}/a_{\rm out}^3$ (see Equations [2] and [A10]). Thus, the evolution of the system with a Solar-mass companion will be very similar to that with a Jupiter-mass companion but 10 times closer, providing an alternative version of the mechanism that may increment the explained pollution rate by accommodating different outer companions.

We note that the presence of a low-mass main sequence star like in the example of Figure 2 would most

[9] Tokovinin & Kiyaeva (2015) find that that the eccentricity distribution for solar-type wide binaries ($a_{\rm b} > 50$ AU) is $f(e_{\rm b}) = 1.2 e_{\rm b} + 0.4$, while $f(e_{\rm b}) = 2 e_{\rm b}$ Kouwenhoven et al. (2007) for very wide binaries ($a_{\rm b} \gtrsim 1000$ AU)

likely be detected had the WD been observed in the first place. However, the fraction of polluted WDs with wide main sequence star companions is small (e.g., Zuckerman 2014). This implies that either the model presented here can only explain a subset of the polluted WDs, or that the current sample of outer companions of polluted WDs is largely incomplete. We briefly discuss the latter alternative, namely, other types of companions might still escape detection and might contribute to the incompleteness of the current sample of companions.

First, outer planetary companions and brown dwarfs at $\sim 10-100$ AU distances can remain undetected (e.g., Farihi et al. 2005; Debes et al. 2011; Day-Jones et al. 2013). Also, these outer companions can drive eccentricities to nearly unity values not only by the KL mechanism (for which large inclinations respect to the planetesimal disk are required), but also by either a nearly coplanar and eccentric body (Li et al. 2014; Petrovich 2015b) or secular chaotic diffusion due to two or more eccentric and/or inclined bodies (Lithwick & Wu 2011; Wu & Lithwick 2011; Batygin et al. 2015).

Second, stellar-mass companions such as other fainter WDs or neutron stars and black holes can also escape detection. One intriguing observational puzzle is the mismatch between the measured binary fraction of WDs ($\sim$ 30%; Farihi et al. 2005; Holberg et al. 2016) and that of their progenitors ($\sim 70-100$%, e.g., Kouwenhoven et al. 2007). As noted by Ferrario (2012), a relatively flat mass ratio distribution for the progenitors of WDs gives a better fit the mass distribution of the detected WDs companions, typically M-dwarfs. However, this same distribution also implies that $\sim$ 30% of the WDs should be in double WD systems, most of them "hiding" as singles. Similarly, based on the completeness of the sample of A-stars in De Rosa et al. (2014), Klein & Katz (2016) argued that $\sim$ 10% of these WD progenitors are likely to host undetected companions that will become WDs within the age of our galaxy. In this picture, current catalogs are typically missing the fainter WDs in the WD-WD system.

### 4.5. *Effects ignored and simplifications*

We discuss some of the relevant effects ignored in this work that might change the dynamics of the system.

*Extra planets in the system*— For simplicity, we have considered a planetary systems with only one planet. We expect our results not to be significantly altered if extra planets within $\sim 1-5$ AU are present in the system (those would also be engulfed). In particular, the extra planets enhance the precession rate of the small bodies in the disk and shield the bodies from outer perturbations at even larger distances (i.e., the Laplace radius in Equation [3] increases[10]).

If one or more distant enough planets do survive the AGB phase, these can quench the secular instabilities and our mechanism would not operate (at least in its cleanest version described here). However, the surviving planets themselves could be susceptible to secular perturbations due to the distant perturber. This effect can, in principle, destabilize a planetary system and/or excite the eccentricities of the planets, and such processes in turn can lead to the tidal disruption of small bodies by the WD.

*Mass loss and galactic tides on the very wide binaries*— For wide enough binaries ($\sim 10^4$ AU), mass loss can happen on timescales that are not too short compared to the orbital timescales and the response of the orbital elements would be different (Veras et al. 2011; Bonsor & Veras 2015) from what is described in Section 2.2. In general, this implies that either the companion becomes more eccentric (or even unbound), which can enhance the eccentric KL mechanism (e.g., Naoz 2016). In addition, these wide binaries will be affected by galactic tides and have their angular momentum altered, which again has the potential of enhancing the secular interactions.

*Stellar evolution*— We have modeled the planetary engulfment by shrinking the orbit in a prescribed way (see Equation 5) to see how the orbital elements of the planetesimal respond to a gradual planet removal. In reality, the process is much more complicated and the radius of the star during the AGB can undergo pulsations, while tides in the star lead to planet inspiral. These effects have been modeled in detail by Mustill & Villaver (2012) and Villaver et al. (2014). Their results indicate that the engulfment generally happens on timescales of $\sim 0.1$ Myr. This timescale is shorter than the shortest secular timescale[11] $\tau_{\rm KL}$ of planetesimals during engulfment for binaries with $a_{\rm b} \gtrsim 100$ AU. Therefore, we expect our model to operate for these wide binaries regardless of the details of planet engulfment.

In a future work, we will calculate the effects of mass loss and the planetary engulfment using realistic stellar evolution models and incorporate these in a population synthesis model. By doing this, we will be able to better address the significance of our model.

## 5. CONCLUSIONS

We have studied a new mechanism to explain the observed metal pollution in white dwarfs through the tidal disruption of small rocky bodies in a planetesimal disk. We propose that one or several planets can shield a planetesimal disk against the KL mechanism due a distant binary companion. Once the host star evolves off the main sequence to become a WD, these planets can be engulfed (most likely during the AGB phase), thus triggering the KL mechanism, and leading to the tidal disruption of the rocky bodies in the planetesimal disk.

We have shown that this mechanism can account for the observed accretion rates for WDs with all cooling ages provided that the disks have masses $\sim 10^{-4}-10^{-2}M_{\oplus}$. Our model allows for planetesimal disks with large radial extents, and as a consequence, it presents the following advantages compared to other models:

- it provides a steady supply of material (each part of the disk has a different and long disruption timescale), enhancing the probability of observing the pollution of WD atmospheres;

[10] By adding $i=1,..,N$ bodies with masses $m_i$ and semi-major axes $a_i$ we just replace $m_{\rm p}a_{\rm p}^2$ by $m_{\rm p}a_{\rm p}^2+\sum_{i=1}^{N} m_i a_i^2$ in the Laplace radius in Equation (3).

[11] The shortest secular timescale can be obtained from evaluating $\tau_{\rm KL}$ in Equation (11) at a semi-major axis and period of a planetesimal located at the Laplace radius in Equation (3).

- it allows for low-density surface disks, which can survive internal disruptive collisions over long timescales.

This mechanism is only triggered after the host star has left the main sequence, providing a self-consistent explanation as to why the KL mechanism does not act on the planetesimal disk for the prior few Gyrs. Our estimates indicate that this model can account for a significant fraction of the polluted WDs. Complete searches for companions of WDs might shed light on the significance of our proposal.

We are grateful to Daniel Tamayo, Dimitri Veras, Dong Lai, Norm Murray, Nicholas Stone, Roman Rafikov, and Yanqin Wu for enlightening discussions. C.P. acknowledges support from the Gruber Foundation Fellowship.

## APPENDIX

## SECULAR EQUATIONS OF MOTION

Consider a mass-less planetesimal orbiting the center of mass of a star with mass $M_s$ and an inner planet with mass $m_p$ (total and reduced masses $M_{\rm in} = M_{\rm s} + m_{\rm p}$ and $\mu_{\rm in} = M_{\rm s}M_{\rm p}/M_{\rm in}$, respectively) with semi-major axis $a$ with eccentricity $e$. The instantaneous Keplerian orbit of this body oriented in space by the eccentricity vector $\mathbf{e}$ and the dimensionless specific angular momentum vector $\mathbf{j} = \sqrt{1-e^2}\,\hat{\mathbf{j}}$. The host star is also a member of a wide binary $M_b$. Thus, the asteroid orbit is perturbed by two non-Keplerian potentials, which we call $\langle\Phi_{\rm in}\rangle$ (due to the star-planet pair, of orbital parameters $a_{\rm in}$ and $e_{\rm in}$) and $\langle\Phi_{\rm out}\rangle$ (due to the distant stellar binary, of orbital parameters $a_{\rm out} = a_b$ and $e_{\rm out} = e_b$). The non-Keplerian potential averaged over all the orbits to octupole order in the semi-major axis ratio and including a term to describe the precession due to General Relativity (GR) is:

$$\Phi = \langle\Phi_{\rm in,quad}\rangle + \langle\Phi_{\rm in,Oct}\rangle + \langle\Phi_{\rm out,quad}\rangle + \langle\Phi_{\rm out,Oct}\rangle + \langle\Phi_{\rm cross,Oct}\rangle + \langle\Phi_{\rm GR}\rangle, \tag{A1}$$

where $\langle\Phi_{\rm cross,Oct}\rangle$ is a cross-term coupling the planetesimal's orbit to both the inner and outer orbits (Hamers et al. 2015). Following the notation of Muñoz & Lai (2015), we write these potentials as:

$$\langle\Phi_{\rm in,quad}\rangle(\mathbf{e},\mathbf{j}) = -\frac{1}{4}\frac{\mathcal{G}M_{\rm in}}{a}\epsilon_{\rm in}(1-e^2)^{-5/2}\Big[(1-6e_{\rm in}^2)(1-e^2) - 3(1-e_{\rm in}^2)(\hat{\mathbf{j}}_{\rm in}\cdot\mathbf{j})^2 + 15e_{\rm in}^2(\hat{\mathbf{e}}_{\rm in}\cdot\mathbf{j})^2\Big], \tag{A2}$$

$$\langle\Phi_{\rm out,quad}\rangle(\mathbf{e},\mathbf{j}) = -\frac{1}{8}\frac{\mathcal{G}M_{\rm in}}{a}\epsilon_{\rm out}(1-e_{\rm out}^2)^{-3/2}\Big[1-6e^2-3(\hat{\mathbf{j}}_{\rm out}\cdot\mathbf{j})^2 + 15(\hat{\mathbf{j}}_{\rm out}\cdot\mathbf{e})^2\Big], \tag{A3}$$

$$\langle\Phi_{\rm in,Oct}\rangle(\mathbf{e},\mathbf{j}) = -\frac{15}{32}\frac{\mathcal{G}M_{\rm in}}{a}\epsilon_{\rm in}\,\epsilon_{\rm in,Oct}(1-e^2)^{-7/2}\times\Bigg\{(\mathbf{e}\cdot\hat{\mathbf{e}}_{\rm in})\Big[(8e_{\rm in}^2-1)(1-e^2) - 35e_{\rm in}^2(\mathbf{j}\cdot\hat{\mathbf{e}}_{\rm in})^2 \tag{A4}$$

$$+ 5(1-e_{\rm in}^2)(\mathbf{j}\cdot\hat{\mathbf{j}}_{\rm in})^2\Big] + 10(1-e_{\rm in}^2)(\mathbf{e}\cdot\hat{\mathbf{j}}_{\rm in})(\mathbf{j}\cdot\hat{\mathbf{e}}_{\rm in})(\mathbf{j}\cdot\hat{\mathbf{j}}_{\rm in})\Bigg\}, \tag{A5}$$

$$\langle\Phi_{\rm out,Oct}\rangle(\mathbf{e},\mathbf{j}) = -\frac{15}{64}\frac{\mathcal{G}M_{\rm in}}{a}\epsilon_{\rm out}\,\epsilon_{\rm out,Oct}\Bigg\{(\mathbf{e}\cdot\hat{\mathbf{e}}_{\rm out})\Big[8e^2-1-35(\mathbf{e}\cdot\hat{\mathbf{j}}_{\rm out})^2 + 5(\mathbf{j}\cdot\hat{\mathbf{j}}_{\rm out})^2\Big] + 10(\mathbf{e}\cdot\hat{\mathbf{j}}_{\rm out})(\mathbf{j}\cdot\hat{\mathbf{e}}_{\rm out})(\mathbf{j}\cdot\hat{\mathbf{j}}_{\rm out})\Bigg\}, \tag{A6}$$

$$\begin{aligned}\langle\Phi_{\rm cross,Oct}\rangle(\mathbf{e},\mathbf{j}) = -\frac{9}{32}\frac{\mathcal{G}M_{\rm in}}{a}\epsilon_{\rm in}\epsilon_{\rm out}\epsilon_{\rm out,Oct}\Bigg\{&2(1-e_{\rm in}^2)(\mathbf{e}\cdot\hat{\mathbf{j}}_{\rm in})(\hat{\mathbf{e}}_{\rm out}\cdot\hat{\mathbf{j}}_{\rm in})\Big[4-5(\hat{\mathbf{e}}_{\rm in}\cdot\hat{\mathbf{j}}_{\rm out})^2\Big]\\
&-10(\hat{\mathbf{e}}_{\rm in}\cdot\hat{\mathbf{e}}_{\rm out})(\hat{\mathbf{e}}_{\rm in}\cdot\hat{\mathbf{j}}_{\rm out})\Big[(1+e_{\rm in}^2)(\mathbf{e}\cdot\hat{\mathbf{j}}_{\rm out}) - (1-e_{\rm in}^2)(\mathbf{e}\cdot\hat{\mathbf{j}}_{\rm in})(\hat{\mathbf{j}}_{\rm in}\cdot\hat{\mathbf{j}}_{\rm out})\Big]\\
&+(\mathbf{e}\cdot\hat{\mathbf{e}}_{\rm out})\Big[-(1-6e_{\rm in}^2) - 10(1-e_{\rm in}^2)(\hat{\mathbf{e}}_{\rm out}\cdot\hat{\mathbf{j}}_{\rm in})^2 - 5(\hat{\mathbf{e}}_{\rm in}\cdot\hat{\mathbf{j}}_{\rm out})^2\Big(5e_{\rm in}^2 - 2(1-e_{\rm in}^2)(\hat{\mathbf{e}}_{\rm out}\cdot\hat{\mathbf{j}}_{\rm in})^2\Big)\\
&-20(1-e_{\rm in}^2)(\hat{\mathbf{e}}_{\rm in}\cdot\hat{\mathbf{e}}_{\rm out})(\hat{\mathbf{e}}_{\rm in}\cdot\hat{\mathbf{j}}_{\rm out})(\hat{\mathbf{e}}_{\rm out}\cdot\hat{\mathbf{j}}_{\rm in})(\hat{\mathbf{j}}_{\rm in}\cdot\hat{\mathbf{j}}_{\rm out}) + 5(1-e_{\rm in}^2)(\hat{\mathbf{j}}_{\rm in}\cdot\hat{\mathbf{j}}_{\rm out})^2\\
&-10(1-e_{\rm in}^2)(\hat{\mathbf{e}}_{\rm in}\cdot\hat{\mathbf{e}}_{\rm out})^2\Big(1-(\hat{\mathbf{j}}_{\rm in}\cdot\hat{\mathbf{j}}_{\rm out})^2\Big)\Big] + 10(\hat{\mathbf{j}}_{\rm in}\cdot\mathbf{e})\Big[(1-e_{\rm in}^2)(\hat{\mathbf{e}}_{\rm in}\cdot\hat{\mathbf{e}}_{\rm out})(\hat{\mathbf{e}}_{\rm out}\cdot\hat{\mathbf{j}}_{\rm in})(\hat{\mathbf{j}}_{\rm in}\cdot\hat{\mathbf{j}}_{\rm out})\\
&+(\hat{\mathbf{e}}_{\rm in}\cdot\hat{\mathbf{e}}_{\rm out})\Big(1-(1-e_{\rm in}^2)(\hat{\mathbf{j}}_{\rm in}\cdot\hat{\mathbf{j}}_{\rm out})^2\Big)\Big]\Bigg\}\ ,\end{aligned} \tag{A7}$$

$$\langle\Phi_{\rm GR}\rangle(\mathbf{e}) = 3\left(\frac{\mathcal{G}M_{\rm in}}{a}\right)^2\frac{1}{c^2\sqrt{1-e^2}}\ . \tag{A8}$$

where the unit vectors $(\hat{\mathbf{e}}_{\rm in}, \hat{\mathbf{j}}_{\rm in})$ and $(\hat{\mathbf{e}}_{\rm out}, \hat{\mathbf{j}}_{\rm out})$ define the orientation of the eccentricity and the angular momentum vectors for the inner and outer orbits, respectively, and we have defined

$$\epsilon_{\rm in} \equiv \frac{1}{2}\left(\frac{\mu_{\rm in}}{M_{\rm in}}\right)\left(\frac{a_{\rm in}}{a}\right)^2 \quad , \tag{A9}$$

$$\epsilon_{\rm out} \equiv \frac{1}{(1-e_{\rm out}^2)^{3/2}}\left(\frac{M_{\rm out}}{M_{\rm in}}\right)\left(\frac{a}{a_{\rm out}}\right)^3 \quad , \tag{A10}$$

$$\epsilon_{\rm out,Oct} \equiv \left(\frac{a}{a_{\rm out}}\right)\frac{e_{\rm out}}{1-e_{\rm out}^2}, \tag{A11}$$

$$\epsilon_{\rm in,Oct} \equiv e_{\rm in}\left(\frac{a_{\rm in}}{a}\right)\sqrt{1-4\mu_{\rm in}/M_{\rm in}} \quad , \tag{A12}$$

which characterize the relative strength of the perturbing potentials for a given $a$.

In our calculations, the planet remains in a low-eccentricity orbit ($e_{\rm in} \ll 1$), which implies that $\epsilon_{\rm in,Oct} \ll 1$. Therefore, the amplitude of $\langle\Phi_{\rm cross,Oct}\rangle$ is much smaller than all the terms of the potential in Equations (A2)-(A6) and can be thus neglected.

The equations of motion for $\mathbf{e}$ and $\mathbf{j}$ can be written as

$$\frac{d\mathbf{j}}{dt} = \frac{1}{\sqrt{\mathcal{G}M_{\rm in}a}}\Big(\mathbf{j}\times\nabla_{\mathbf{j}}\Phi + \mathbf{e}\times\nabla_{\mathbf{e}}\Phi\Big) \tag{A13}$$

$$\frac{d\mathbf{e}}{dt} = \frac{1}{\sqrt{\mathcal{G}M_{\rm in}a}}\Big(\mathbf{j}\times\nabla_{\mathbf{e}}\Phi + \mathbf{e}\times\nabla_{\mathbf{j}}\Phi\Big) \tag{A14}$$

In turn, the background system of star, planet, and companion (which is unaffected by the presence of the massless particle) evolves according to the secular dynamics of triple systems. In what follows, we only write the equations of motion for the inner star-planet pair as the outer stellar binary remains roughly fixed during the evolution of the system (i.e., $\mathbf{e}_{\rm out}$ and $\mathbf{j}_{\rm out}$ are roughly constant). Similar to the case of the planetesimal's orbit, we write the non-Keplerian potential of the inner system as:

$$\Phi_{\rm in} = \langle\Phi_{\rm in-out,Quad}\rangle + \langle\Phi_{\rm in-out,Oct}\rangle + \langle\Phi_{\rm in,GR}\rangle, \tag{A15}$$

where

$$\langle\Phi_{\rm in-out,Quad}\rangle(\mathbf{e}_{\rm in},\mathbf{j}_{\rm in}) = -\frac{1}{8}\frac{\mathcal{G}M_{\rm in}}{a_{\rm in}}\mu_{\rm in}\frac{(M_{\rm out}/M_{\rm in})\,(a_{\rm in}/a_{\rm out})^3}{(1-e_{\rm out}^2)^{3/2}}\Big[(1-6e_{\rm in}^2) - 3(\mathbf{j}_{\rm in}\cdot\hat{\mathbf{j}}_{\rm out})^2 + 15(\mathbf{e}_{\rm in}\cdot\hat{\mathbf{j}}_{\rm out})^2\Big] \quad , \tag{A16}$$

$$\langle\Phi_{\rm in-out,Oct}\rangle(\mathbf{e}_{\rm in},\mathbf{j}_{\rm in}) = -\frac{15}{64}\frac{\mathcal{G}M_{\rm in}}{a_{\rm in}}\mu_{\rm in}\,(M_{\rm out}/M_{\rm in})\,(a_{\rm in}/a_{\rm out})^4\,\sqrt{1-4\mu_{\rm in}/M_{\rm in}}\frac{e_{\rm out}}{(1-e_{\rm out}^2)^{5/2}}$$
$$\times\left\{(\mathbf{e}_{\rm in}\cdot\hat{\mathbf{e}}_{\rm out})\times\Big[(8e_{\rm in}^2-1) - 35(\mathbf{e}_{\rm in}\cdot\hat{\mathbf{j}}_{\rm out})^2 + 5(\mathbf{j}_{\rm in}\cdot\hat{\mathbf{j}}_{\rm out})^2\Big] + 10(\mathbf{j}_{\rm in}\cdot\hat{\mathbf{e}}_{\rm out})(\mathbf{e}_{\rm in}\cdot\hat{\mathbf{j}}_{\rm out})(\mathbf{j}_{\rm in}\cdot\hat{\mathbf{j}}_{\rm out})\right\} \quad , \tag{A17}$$

$$\langle\Phi_{\rm in,GR}\rangle = 3\mu_{\rm in}\left(\frac{\mathcal{G}M_{\rm in}}{a_{\rm in}}\right)^2\frac{1}{c^2\sqrt{1-e_{\rm in}^2}} \tag{A18}$$

The equations of motion for $\mathbf{e}_{\rm in}$ and $\mathbf{j}_{\rm in}$ can be written as

$$\frac{d\mathbf{j}_{\rm in}}{dt} = \frac{1}{\sqrt{\mathcal{G}M_{\rm in}a_{\rm in}}}\Big(\mathbf{j}_{\rm in}\times\nabla_{\mathbf{j}_{\rm in}}\Phi_{\rm in} + \mathbf{e}_{\rm in}\times\nabla_{\mathbf{e}_{\rm in}}\Phi_{\rm in}\Big), \tag{A19}$$

$$\frac{d\mathbf{e}_{\rm in}}{dt} = \frac{1}{\sqrt{\mathcal{G}M_{\rm in}a_{\rm in}}}\Big(\mathbf{j}_{\rm in}\times\nabla_{\mathbf{e}_{\rm in}}\Phi_{\rm in} + \mathbf{e}_{\rm in}\times\nabla_{\mathbf{j}_{\rm in}}\Phi_{\rm in}\Big). \tag{A20}$$

We incorporate the effect from mass loss and engulfment of the planet due to tides on the star as:

$$\frac{\dot{a}_{\rm in}}{a_{\rm in}} = -\frac{\dot{M}_s}{M_{\rm in}} - \tau_a^{-1} \equiv \tau_{\rm ml}^{-1}\frac{M_s}{M_{\rm in}} - \tau_a^{-1}, \tag{A21}$$

while we only prescribe the orbit expansion due to mass loss for the planetesimal and outer (binary) orbits as

$$\frac{\dot{a}}{a} = \tau_{\rm ml}^{-1} \quad \text{and} \tag{A22}$$

$$\frac{\dot{a}_{\rm out}}{a_{\rm out}} = \tau_{\rm ml}^{-1}\frac{M_s}{M_s + M_{\rm out}} \tag{A23}$$

respectively.

REFERENCES


Agol, E. 2011, ApJL, 731, L31
Alonso R., Rappaport S., Deeg H. J., Palle E. 2016, A&A,589, L6
Anderson, K. R., Storch, N. I., & Lai, D., 2016, MNRAS, 456, 3671
Antognini, J. M. O. 2015, MNRAS, 452, 3610
Batygin, K., Morbidelli, A., & Tsiganis, K. 2011, A&A, 533, A7
Batygin, K., Morbidelli, A., & Holman, M.J., 2015, ApJ, 799, 120
Bilíková, J., Chu, Y.-H., Gruendl, R. A. et al. 2012, ApJS, 200, 3
Bonsor, A., Mustill, A. J., & Wyatt, M. C. 2011, MNRAS, 414, 930
Bonsor, A., & Veras, D. 2015, MNRAS, 451,1
Bonsor, A., & Wyatt, M. 2010, MNRAS, 409, 1631
Chayer, P., Fontaine, G., & Wesemael, F., 1995, ApJS, 99, 189
Clayton, G.C., De Marco, O. , Nordhaus, J. et al. 2014, AJ, 147, 142
Day-Jones, A. C., Marocco, F., Pinfield, D. J., et al. 2013, MNRAS, 430, 1171
De Rosa, R. J., Patience, J., Wilson, P. A., et al. 2014, MNRAS, 437, 1216
De Ruyter, S., Van Winckel, H., Maas, T., et al. 2006, A&A, 448, 641
Debes, J. H., & Sigurdsson, S. 2002, ApJ, 572, 556
Debes, J. H., Hoard, D. W., Wachter, S., Leisawitz, D. T., & Cohen, M. 2011, ApJS, 197, 38
Debes, J.H., Walsh, K.J., & Stark, C. 2012, ApJ, 747, 148
Farihi J., Becklin E. E., & Zuckerman B., 2005, ApJS, 161, 394
Farihi, J., Gänsicke, B. T., & Koester, D., 2013, Science, 342, 218
Farihi, J. 2016, NewAR, 71, 9F
Ferrario L., 2012, MNRAS, 426, 2500
Fontaine, G., & Michaud, G., 1979, ApJ, 231, 826
Frewen, S. F. N., & Hansen, B. M. S. 2014, MNRAS439, 2442
Gänsicke, B. T., Koester D., Farihi J.,et al. 2012, MNRAS, 424, 333
Gänsicke, B. T., Aungwerojwit, A., Marsh T. R., et al. 2016,ApJL, 818, L7
Gladman, B. 1993, Icarus, 106, 247
Goodwin, S. P. 2013, MNRAS, 430, 6
Koester, D. 2009, A&A, 498, 517
Koester, D., Gänsicke, B. T., & Farihi, J. 2014, A&A, 566, A34
Kouwenhoven, M. B. N., Brown, A. G. A., Portegies Zwart, S. F., & Kaper, L. 2007, A&A, 474, 77
Hadjidemetriou, J. D. 1963, Icarus, 2, 440
Hamers, A. S., Perets, H. B., Antonini, F., & Portegies Zwart, S. F. 2015, MNRAS, 449, 4221
Hamers, A. S., & Portegies Zwart, S. F. 2016, MNRAS, 462, L84
Heng, K., & Tremaine, S. 2010, MNRAS, 401, 867
Holberg, J. B., Oswalt, T. D., Sion, E. M., & McCook, G. P., 2016, (arXiv:1606.01236)
Holman, M., Touma, J., & Tremaine, S. 1997, Nature, 386, 254
Hurley, J. R., Pols, O. R., & Tout, C. A. 2000, MNRAS, 315, 543
Johnson, J. A., Aller, K. M., Howard, A. W., & Crepp, J. R. 2010, PASP, 122, 905
Jura, M., & Young, E. D. 2014, AREPS, 42, 45
Klein, Ygal & Katz, Boaz 2016, arXiv: 1609.03580
Koester, D., Gänsicke, B. T., & Farihi, J. 2014, A&A, 566, A34
Landau, L. D., & Lifshitz, E. M. 1969, Course of Theoretical Physics, Oxford: Pergamon Press, 1969, 2nd ed.
Li, G., Naoz, S., Kocsis, B., & Loeb, A. 2014, ApJ, 785, 116
Lidov, M. L. 1962, Planet. Space Sci., 9, 719
Lithwick, Y. & Wu, Y. 2011, ApJ, 739, 31
Liu, B., Muñoz, D. J., & Lai, D. 2015, MNRAS, 447, 747
Luo L., Katz B., & Dong S. 2016, MNRAS, 458, 3060
Kozai, Y. 1962, AJ, 67, 591
Kratter, K. M., & Perets, H. B. 2012, ApJ, 753, 91
Muñoz, D. J., & Lai, D. 2015, Proceedings of the National Academy of Science, 112, 9264
Muñoz, D. J., Lai, D. , & Liu, B. 2016, MNRAS, 460, 1086
Mustill, A. J., Veras, D., & Villaver, E. 2014, MNRAS, 437, 1404
Mustill, A. J., & Villaver, E. 2012, ApJ, 761, 121
Naoz, S., Farr, W. M., & Rasio, F. A. 2012, ApJ, 754, L36
Naoz S., 2016, arXiv:1601.07175
Peter, D., Feldt, M., Henning, Th., Hormuth F. 2012, A&A, 538, 74
Petrovich, C. 2015, ApJ, 799, 27
Petrovich, C. 2015b, ApJ, 805, 75
Rafikov, R. R. 2013, ApJ, 765, L8
Raghavan, D., McAlister, H. A., Henry, T. J., et al. 2010, ApJS, 190, 1
Rappaport, S., Gary, B. L., Kaye, T., et al. 2016, MNRAS, 458, 4
Rein, H., & Liu, S. F. 2012, A&A, 537, A128
Rein, H., & Spiegel, D. S. 2015, MNRAS, 446, 1424
Takeda G., Kita R., & Rasio F. A., 2008, ApJ, 683, 1063
Tamayo D., Burns J. A., Hamilton D. P., Nicholson P. D., 2013, AJ, 145, 54
Tamayo, D., Triaud, A. H. M. J., Menou, K., & Rein, H. 2015, ApJ, 805, 100
Tokovinin, A. & Kiyaeva, O. 2015, arXiv:1512.00278
Tremaine S., Touma J., Namouni F., 2009, AJ, 137, 3706
Tremaine, S., & Yavetz, T. D. 2014, American Journal of Physics, 82, 769
Van Winckel, H., Lloyd Evans, T., Briquet, M., et al. 2009, A&A, 505, 1221
Vanderburg, A., Johnson ,J. A., & Rappaport, S., 2015, Nature, 526, 546
Veras, D. 2016, R. Soc. open sci., 3,150571
Veras, D., Evans, N. W., Wyatt, M. C., & Tout, C. A. 2014a, MNRAS, 437, 1127
Veras, D., & Gänsicke, B. T. 2015, MNRAS, 447, 1049
Veras, D., Leinhardt, Z. M., Bonsor, A., & Gänsicke, B. T. 2014b, MNRAS, 445, 2244
Veras, D., Leinhardt, Z. M., Eggl, S., & Gänsicke, B. T. 2015, MNRAS, 451, 3453
Veras, D., Mustill, A. J, Bonsor, A., & Wyatt, M. C. 2013, MNRAS, 431, 1686
Veras, D., Wyatt, M. C., Mustill, A. J., Bonsor, A., & Eldridge, J. J. 2011, MNRAS, 417, 2104
Villaver, E., Livio, M., Mustill, A. J., & Siess, L. 2014, ApJ, 794, 3
Winn, J. N., & Fabrycky, D. C. 2015, Annual Review of Astronomy and Astrophysics, 53, 409
Wu, Y. & Lithwick, Y. 2011, ApJ, 735,109
Wyatt M. C., Smith R., Greaves J. S., Beichman C. A., Bryden G., Lisse C. M., 2007, ApJ, 658, 569
Wyatt M. C., Farihi J., Pringle J. E., Bonsor A., 2014, MNRAS, 439, 3371
Xu S., Jura M., Dufour P., & Zuckerman B. 2016, ApJL, 816,L22
Zuckerman B., Koester D., Melis C., et al. 2007, ApJ, 671, 872
Zuckerman, B., Koester, D., Reid, I. N., & Hünsch, M. 2003, ApJ, 596, 477
Zuckerman, B., Melis, C., Klein, B., Koester, D., & Jura, M. 2010, ApJ, 722, 725
Zuckerman B., 2014, ApJ, 791, L27